We are IntechOpen, the world's leading publisher of Open Access books Built by scientists, for scientists

6,900
Open access books available

185,000
International authors and editors

200M
Downloads

Our authors are among the

154
Countries delivered to

TOP 1%
most cited scientists

12.2%
Contributors from top 500 universities



WEB OF SCIENCE™

Selection of our books indexed in the Book Citation Index in Web of Science™ Core Collection (BKCI)

Interested in publishing with us?
Contact book.department@intechopen.com

Numbers displayed above are based on latest data collected.
For more information visit www.intechopen.com



21

Magnetic Induction Heating of Nano-sized Ferrite Particles

Yi. Zhang[1] and Ya. Zhai[1,2]
[1]*Department of Physics, Southeast University, Nanjing 211189,*
[2]*The center of Material Analysis, National Laboratory of Solid Microstructures, Nanjing University, Nanjing 210093,*
China

1. Introduction

Magnetic nano-structured materials have attracted much attention due to their unique properties and potential applications. Magnetic induction heating behavior in magnetic particles provides a benefit for biomedical applications, such as targeted drug delivery[1, 2], diagnostics[3], and magnetic separation[4, 5]. The magnetic nano-structured materials are also being explored as contrast agents in MRI[6, 7], thermo responsive drug carriers[8], and the hyperthermia[9, 10]. Hyperthermia is a promising approach for the thermal activation therapy of tumor[10, 11]. Inevitable technical problems for hyperthermia are the difficulty of heating only the local tumor to the intended temperature without damaging much of the surrounding healthy tissue and precise control of temperature. Induction heating of magnetic nanoparticles in an alternating field can solve the above problems with their unique characters of self-heating, self-temperature controlling due to the magnetic loss in AC magnetic field. In addition, nanoparticles can be conveniently transported to the local region of tumor tissue by the interventional techniques.

Magnetic particles heat inductively due to magnetic losses associated with the magnetization/demagnetization cycling. Ferrites (magnetic iron oxides) nanoparticles, are good candidates for Hyperthermia tumor therapy due to their excellent high-frequency response and high resistivity property, especially the possible large magnetic loss and high heating ability. Among them, Fe_3O_4 particles have attracted much interests because they are considered as a material with non-toxicity and biological compatibility due to their main composition of Fe ions. Besides, it is well known that Zn additives in magnetic oxides can change the final heated temperature and Zn is also an element in people's favor. In this chapter, we will introduce the magnetic induction heating behaviors of ferrite nanomaterials and fluid in following three aspects: (1) Basic knowledge of magnetic induction heating in ferrite nano-materials. (2) The effect of magnetic field and frequency on heating efficiency and speed. (3) Magnetic fluid hyperthermia behaviors.

2. Basic knowledge of magnetic induction heating of ferrite nano- materials

The magnetic induction heating of ferrite materials is originated from their power loss in alternating magnetic field. The total power loss (P_L) is composed of three parts, hysteresis

loss (P_h), eddy current loss (P_e) and residual loss (P_r) [12, 13]. Hysteresis loss is due to the irreversible magnetization process in AC magnetic field. Eddy current loss is the Joule loss due to eddy current induced by the alternating magnetic field and hence depends much on the electrical resistivity of the material. The physical origin of residual loss is more complicated. The residual loss cannot be separated straight forwardly from eddy current loss, nor even from hysteresis loss easily. However, most ferrite materials have higher electrical resistivity, leading to very low eddy current loss. Thus the magnetic induction heating of ferrite materials is mainly caused by the hysteresis loss and residual loss in alternating magnetic field. The residual loss is originated from various relaxation effects of magnetization in magnetic field. Thus it is also called relaxation loss. In some low loss ferrites the relaxation effect shows resonance at certain high frequencies.

The hysteresis loss refers to the loss due to irreversible magnetization process in AC field. In DC field a hysteresis loop is observed during magnetization reversal for one cycle when the field is not very low. The hysteresis loss for one cycle can be easily estimated from the area of the hysteresis loop, W_h and the power loss is expressed as $P_h=W_h f$, where f is frequency. Note that the irreversible process and the hysteresis loop changes with the amplitude and frequency of the AC field. When the amplitude of the AC field increases, the H_c and B_r increase and hysteresis loss increases until the maximum value. However, when the frequency increases, the hysteresis loss due to irreversible process decreases and disappears at a high frequency when the irreversible process cannot catch the fast changing AC field. Nevertheless, an AC hysteresis loop can still be observed experimentally which is due to time lag of magnetization cause by after effect or relaxation effect relative to AC field. For bulk ferrites the hysteresis loss may disappear when the frequency is above MHz[14]. For induction heating, the frequency is generally not very high with relatively high field amplitude, thus the hyteresis loss often may still exist and makes the main contribution.

For low frequency(f <1kHz)and small amplitude of AC field (H<<H_c, M<M_s/10), the early studies by Jordan[15] and Legg[16] lead to the following well known expression for the losses of magnetic material in AC magnetic field:

$$W / B_m{}^2 = aB_m + ef + c \tag{1}$$

Here B_m is the amplitude of the magnetic induction in the material. The first term refers to magnetic hysteresis loss with a the coefficient of magnetic hysteresis loss. Second term stands for eddy loss which is proportional to the frequency of AC field with e the coefficient of eddy loss. The third term represents residual loss which is almost a constant in a low frequency for metals. However for ferrites c is found to be dependent on frequency so that it should be noted not to be confused with eddy current loss. .. Thus equation (1) should be changed to the following for ferrites:

$$W / B_m{}^2 = aB_m + ef + c(f) \tag{2}$$

When the amplitude of magnetic field is small, within so called "Rayleigh" region, the magnetic hysteresis loss per cycle can be expressed by

$$W_h = \frac{4}{3}\mu_0 b H_m{}^3 = \mu_0 \pi \mu'' f H_m{}^2 \tag{3}$$

Here b is so called Rayleigh constant indicating a linear dependence of permeability on H, namely $\mu=\mu_i+bH$ in Rayleigh region. When the amplitude of magnetic field is highrt than that in Rayleigh region the hysteresis loss can only be determined empirically.

For nano-sized magnetic particles, the eddy currnt loss can be calculated without considering the effect of skin depth by assuming uniform distribution of magnetic field in the particle. The calculated eddy current power loss of the spherical particles is expressed by the following expression[14],

$$P_e = \frac{\pi}{20} B_m{}^2 d^2 \sigma f^2 [10^{-10} w / cm^2] \tag{4}$$

in CGS unit, where d is the diameter of the particle and $\sigma$is the conductivity. P_e is generally very small in ferrite materials. The mechanism of residual loss is complicated and the constant c can only be determined from experiment.

Earlier study for NiZn ferrite material reported that the magnetic hysteresis loss is dominant and for very soft MnZn ferrite material, in which the hysteresis loss is low and residual loss is dominant[17].

For medium and strong magnetic field and low frequency, The power loss was proved by experiment as blow[17]:

$$P = P_h + P_e = \eta B_m{}^n f + eB_m^2 f^2 \tag{5}$$

Here the constants η,and n for magnetic hysteresis loss are determined empirically. For Fe sheet, n was found to be 1.6. The coefficient e for eddy loss has been calculated theoretically in different cases.

For high frequency AC field, the magnetic loss is difficult to separate since the total loss P is not linear with f and the three components in equation (2) are all frequency dependent and have interaction among them.

As the size of the ferrite particle is larger than the critical size of single domain, the particle may contain several domains with domain walls between the adjacent domains. The magnetization reversal and hysteresis loss are realized by irreversible domain wall displacement. When the size of ferrite particle approaches the critical size of single domain, the magnetization reversal and hysteresis loss are realized by irreversible domain rotation in overcoming the energy barrier $E= KV$, where K is the anisotropy constant and V is the volume of the magnetic particle. Generally speaking, H_c and hysteresis loss due to irreversible domain wall displacement is smaller than that due to irreversible domain rotation. When the amplitude of AC field is large enough the hysteresis loss due to irreversible domain rotation dominates for single domain particles. When the particle size is smaller than the single domain critical value the superparamagnetic behavior appears, in which the thermal agitation helps the magnetization reversal to overcome the energy barrier. Then H_c is smaller and the hysteresis loss is smaller and down to zero for completes superparamagnetic tiny particles. Therefore the induction heating is optimized by selecting ferrite composition, particle size, AC field intensity and frequency.

For the superparamagnetic ferrite nano-materials in carrier liquid, induction heating can be due to either so-called Neel relaxation process or rotational Brownian motion within a carrier liquid, or to both generally. The Neel relaxation process refers to the heat assisted domain rotations in the particles by the AC magnetic field as mentioned above. The Browing relaxation refers to the rotation of the magnetic particle as a whole because of the

torque exerted on the magnetic moment by the external AC magnetic field, and the energy barrier for reorientation of a particle is determined by rotational friction in the surrounding liquid. In general, the heating effects usually proceed via one of the two mechanisms: Neel and Brownian relaxation processes, or via both together. The total relaxation losses due to both processes could be calculated by the following equation[18]

$$P = (mH\omega\tau_{eff})^2 / [2\tau_{eff}\kappa TV(1+\omega^2\tau^2{}_{eff})] \quad (6)$$

Here, m is the particle magnetic moment, ω is the AC field frequency, H is the ac field amplitude, V is the nanoparticle volume, and τ_{eff} is the effective relaxation time. When the ac magnetic field is applied to magnetic nanoparticles, their magnetic moments attempt to rotate following the magnetic field with time lag. The effective relaxation time (τ_{eff}) is given by [19]

$$\tau_{eff} = \frac{\tau_B \tau_N}{\tau_B + \tau_N} \quad (7)$$

in which the Brownian relaxation is

$$\tau_B = 3\eta V_H / kT \quad (8)$$

where η is the viscosity of the carrier fluid, k is the Boltzmann constant, T is the absolute temperature, and V_H is the hydrodynamic volume of the particle. Néel relaxation is

$$\tau_N = \tau_0 \exp(KV / kT) \quad (9)$$

where τ_0 is on the order of 10^{-9} S, and K is the anisotropy constant of the magnetic nanoparticle.

The Curie temperature (T_c) of the material provides a self-temperature- limiting behavior. Below T_c , the magnetic material exhibits the magnetic order and above T_c , it becomes paramagnetic (magnetic disorder) which does not show magnetic hysteresis. The magnetic material is heated up efficiently in an alternating magnetic field until it reaches its T_c, above which the material becomes paramagnetic and the heating effect almost stops. Then when temperature is cooled down below T_c, the nano-particles resume the strong magnetic state and heat up again and thus stay around T_c. Therefore the magnetic induction heating has a final equilibrium temperature, called dwell temperature, and we can control the temperature by changing T_c in terms of doping some impurities in magnetic particles. For Curie temperature-controlled heating, magnetic heat generation must greatly exceed other mechanisms of heat generation, thus the magnetic material will heat efficiently in an induction field until it reaches its T_c. Whereas T_c can be adjusted by changing the composition of ferrites. Examples are magnetite with a wide range of Zn substitution [20].

It is well-known that the Curie point T_c will drop as a result of the substitution of Zinc owing to the reduced A-B exchange interaction with increasing Zn content in the case of mixed Zn ferrites with spinel structure, $Me_{1-\delta}Zn_{\delta}Fe_2O_4$. Since the Curie temperature T_c decreases from 680°C to 0°C with increasing Zn content, the dwell temperature of various spinel structured ferrite particles under the AC field could be controlled by Zn substitution.

We have investigated the self-heating and self-temperature-limiting behavior tests of three series of $Zn_xFe_{3-x}O_4$, $Ni_{1-x}Zn_xFe_2O_4$ and $Co_{1-x}Zn_xFe_2O_4$ ferrite nano-particles with various Zn

substitutions. The particles size of various Zn ferrites decreases from 23 nm to 6 nm with increasing Zn contents. By comparing the dwell temperature of various Zn ferrites nano-particles of the same weight of 2.0 g with their T_c, we obtained that the dwell temperature in AC field with 72kHz and 54.3mT is close to the Curie temperature T_c as shown in Fig.1. We see that the T_c does decrease with increasing Zn content in the spinel structured ferrite nano-materials. The final heating temperature is clearly determined by the Curie temperature of the material and is always slightly lower than its Curie point. This deviation is most likely due to heat losses to the environment, which are balanced by the small amount of heat which the material generates immediately below its Curie temperature. These environmental losses have been estimated based on the cooling rates of the samples after removal from the induction field, and are used to provide a minor correction in all subsequent quantitative calculations of induction heat generation.

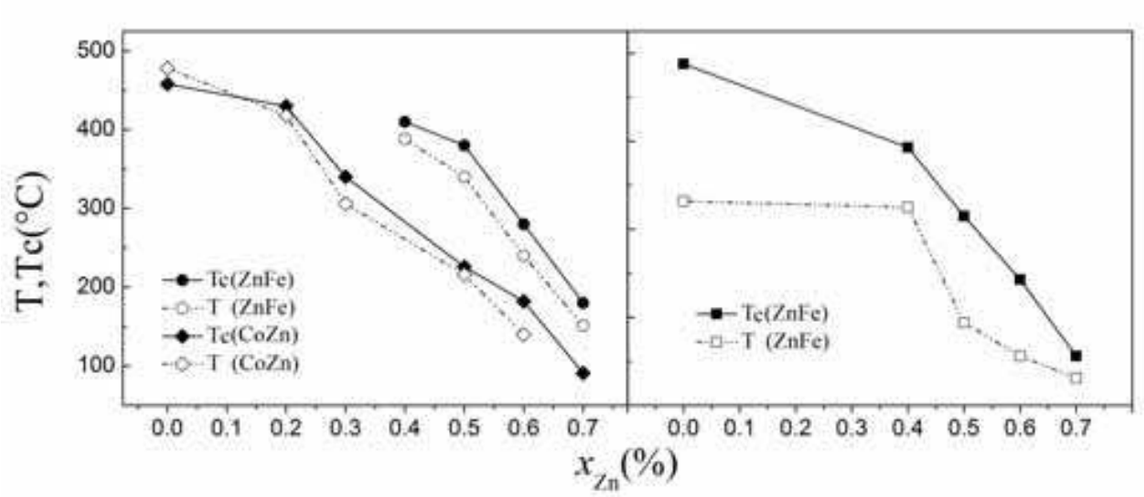


Fig. 1. The dwell temperature and T_c of Zn content of ferrite nano-particles

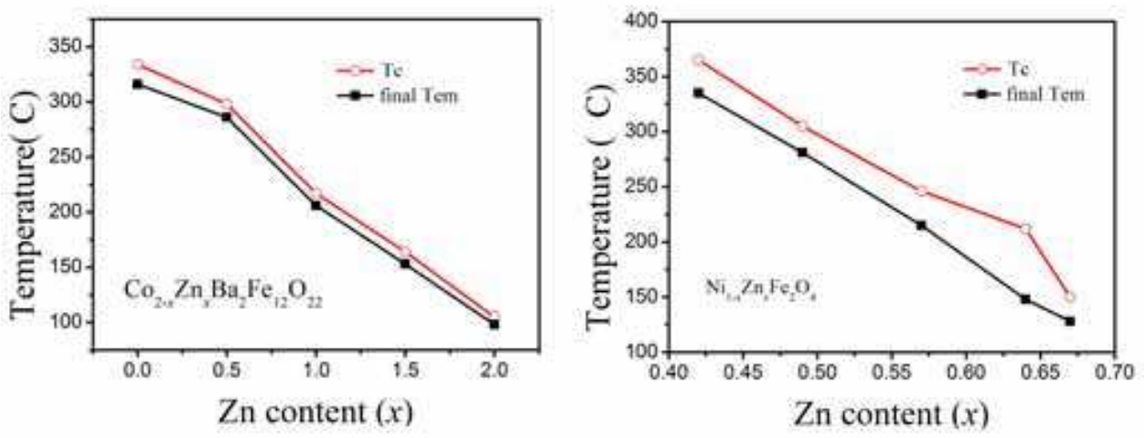


Fig. 2. The dwell temperature T and T_c in higher frequency(5.85 MHz)[21]

Similar results can be found in AC field with higher frequency[21]. John Xiao group investigated the Curie temperature-controlled induction heating behavior of $Co_2Ba_2Fe_{12}O_{22}$ semihard ferrites and $NiFe_2O_4$ soft ferrites in AC field with 5.85 MHz and 50–500 Oe,

respectively. In scanning electron microscopy images, particle sizes of final products are in several microns range (average 2.52 μm for $Co_{1.5}Zn_{0.5}Ba_2Fe_{12}O_{22}$ and 2.85 μm for $Ni_{0.51}Zn_{0.49}Fe_2O_4$).

It is interesting to note that for Zn-ferrite particles, the change tendency of final dwell temperature with different Zn content in the ac field with both 72kHz and 5.85MHz is similar.

3. The effect of magnetic field intensity and frequency on heating efficiency and speed

With regard to the electromagnetic devices used for magnetic induction heating, the technology of AC magnetic field is still under development. Most of magnetic magnetic induction heating experiments are performed with laboratory-made generators in the frequency range of 50 kHz to 10MHz, with magnetic field amplitudes up to few tens of mT, using an induction coil (Fig.3) or in the air-gap of a magnetic inductor, which are also used in our experiments.

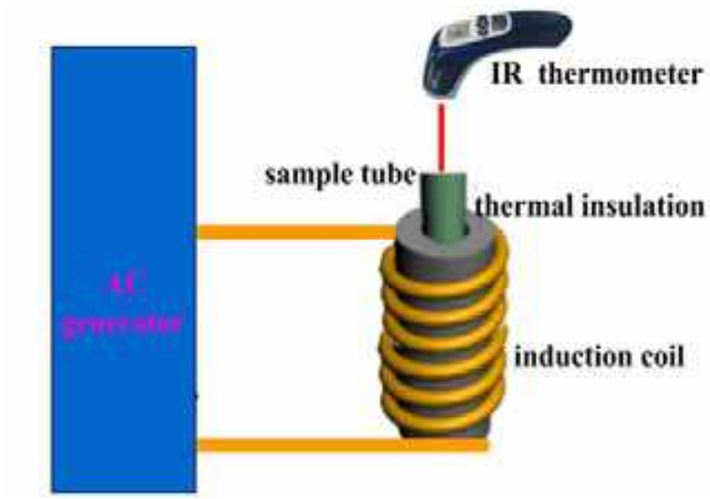


Fig. 3. Schematic diagram of a typical laboratory- made magnetic heating device

There are two kinds of sensor for detecting temperature including contact and non-contact type. The contact temperature sensor is usually thermistance. It is cheaper but poor reliability, and it required the circuit for signal treatment. We recommend DS18B20 digital temperature sensor made by DALLAS Company we have used, which is appropriate for detecting the heating temperature of magnetic liquid due to its wider temperature detecting range from -55°C to 125 °C and higher temperature resolution of 0.0625°C. In addition, DS18B20 digital temperature sensor has many advantages of smaller volume, stronger anti-jamming ability and easy connection with the microprocessor [22]. Such contact type sensor is suitable to measure the temperature of the ferrofluid. Two kinds of non-contact type temperature sensor were usually used, optical fiber and infrared ray sensor. The former should be more accurate than later, both are appropriate for detecting the heating temperature of naked materials.

In our experiment, a fundamental, quantitative understanding of the heating mechanisms in the presence of an induction field, whose frequency and intensity are typically 72kHz and 0-

60 mT, respectively, have been investigated on three series of spinel structured ferrites: ZnFe ferrite ($Zn_xFe_{3-x}O_4$, x = 0~0.8), NiZn ferrite ($Ni_{1-x}Zn_xFe_2O_4$, x=0~0.7) and CoZn ferrite ($Co_{1-x}Zn_xFe_2O_4$, x =0~0.8). Different level of Zn substitution allows a systematic variation in Curie temperature, from 100 to 480 °C. Both materials were synthesized using a chemical co-precipitation method. The chemical reaction equation is as follows:

$$xZn^{2+}+(1-x)M^{2+}+2Fe^{3+}+8OH^{-}\rightarrow Zn_xM_{1-x}Fe_2O_4+4H_2O,\ M = Fe, Ni, Co$$

The compositions of various ferrite particles were determined by EDS, the structures were analyzed by XRD and the particle size were measured by TEM and XRD listed in Table 1.

x	size of particles (nm)		
	$Zn_xFe_{3-x}O_4$	$Ni_{1-x}Zn_xFe_2O_4$	$Co_{1-x}Zn_XFe_2O_4$
0	16	12	9
0.2	16	-	9
0.3	-	23	-
0.4	15	23	8
0.5	13	23	-
0.6	-	17	6
0.7	-	15	-
0.8	11	-	6

Table 1. The composition and the size of 3 kinds of ferrite nano-particles

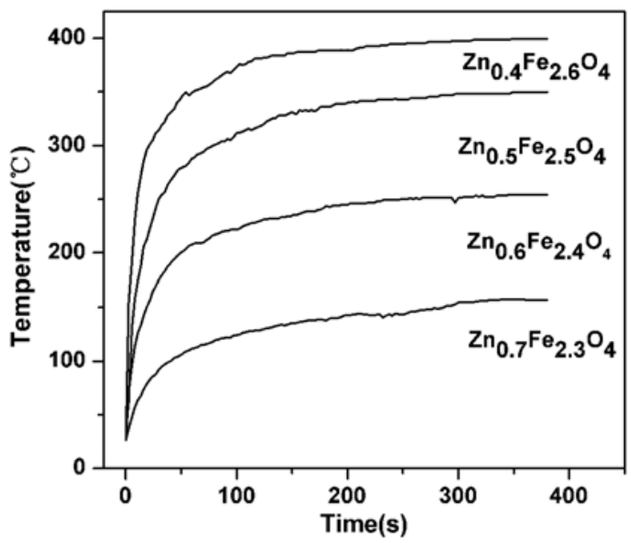


Fig. 4. The induction heating curves of $Zn_xFe_{3-x}O_4$ ferrite nanoparticles in ac field intensity with a frequency of 71 KHz and a intensity of 54.3mT.

Fig.4 shows the induction heating curves of $Zn_xFe_{3-x}O_4$ ferrite nanoparticles in ac field with a frequency of 71 KHz and an intensity of 54.3mT. It is seen that the heating temperature

increases with increasing time and reaches equilibrium basically after 100-200 seconds. The dwell temperature can be obtained by extrapolating from linear part of the curve to 0 second. From Fig.4, we see the dwell temperature increases with decreasing Zn content. If we define a heating rate as $\Delta T/\Delta t$, the heating rate also increases with decreasing Zn additives. Same result of $Co_{1-x}Zn_xFe_2O_4$ is shown in Fig.5, the dwell temperature and heating rate increase with deceasing Zn content. However, for $Ni_{1-x}Zn_xFe_2O_4$, the dwell temperature and heating rate show different behaviors. The highest dwell temperature and heating rate appear at the Zn concentration of 0.5, which is the composition of largest magnetization. Also, the heating rate of $Co_{1-x}Zn_xFe_2O_4$ ferrets is obviously faster than that of $Ni_{1-x}Zn_xFe_2O_4$, which might be due the larger magnetic hysteresis loop area of the former than the latter.

The effect of AC magnetic field with fixed frequency of 72kHz and different amplitude on magnetic induction heat behavior of three Zn ferrite nano-materials has been studied. Fig.6 shows the heating curve of $Co_{0.8}Zn_{0.2}Fe_2O_4$ ferrite nanoparticles in different intensity of ac

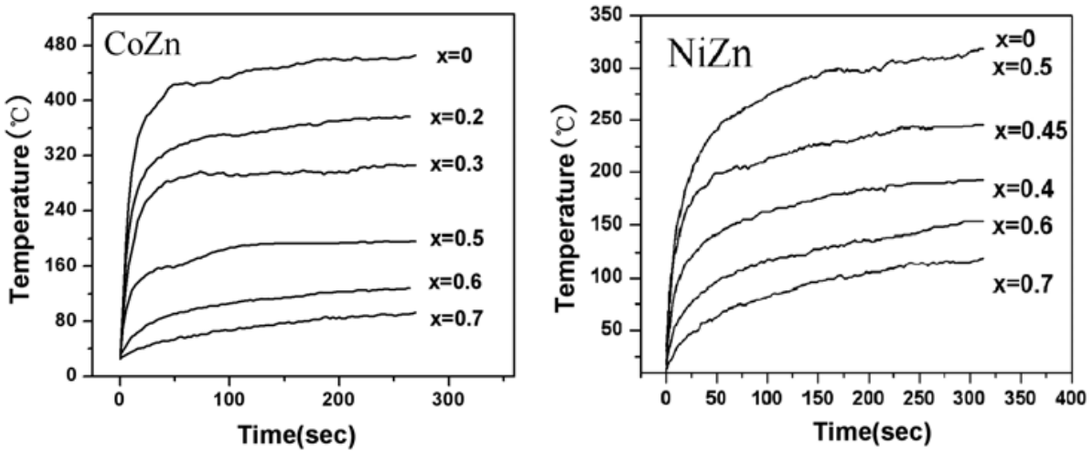


Fig. 5. The induction heating curves of $Ni_{1-x}Zn_xFe_2O_4$ and $Co_{1-x}Zn_xFe_2O_4$ ferrite nanoparticles in ac field with a frequency of 71 KHz and an intensity of 41.1mT.

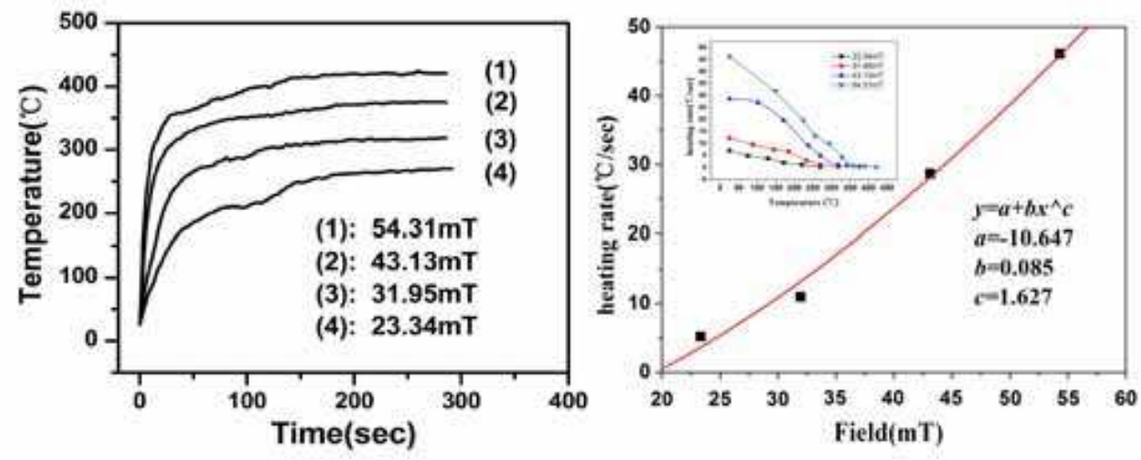


Fig. 6. The hearting curve of $Co_{0.8}Zn_{o.2}Fe_2O_4$ ferrite nanoparticles in different intensity of ac magnetic field (left) and the hearting rate as a function of amplitude of ac fields.

magnetic field and the heating rate as a function of amplitude of ac field. From Fig.6, we see that the dwell temperature and heating rate increase with increasing ac field (left) and the heating rate in different AC fields decreases as the temperature rises monotonously (inset). Fig.6 (right) shows the induction heating rate (when the temperature rise from room temperature to 100°C) as a function of field intensity, for $Co_{0.8}Zn_{0.2}Fe_2O_4$ ferrite. It is noted that the heating rate is approximately proportional to $H^{1.6}$.

For ferrites with the high resistivity eddy current has little contribution to heating. We assume that heat generation basically comes from hysteresis loss. The heat generation from hysteresis is given by [23]

$$\bar{C}_p m\,(dT/dt) = Q_{generation} = c_1 f W_h\,, \tag{9}$$

where in the ideal case, c_1=1. W_h refers to magnetic hysteresis loss for medium and strong magnetic field. Thus the expression of heating rate is

$$\frac{dT}{dt} = \frac{c_1}{C_p m} f W_h = \frac{c_1}{C_p m} f B_m^{1.6} \tag{10},$$

which just agrees well with our experimental results.

Comparing with higher frequency studied by John Xiao group[21], heating rates increase dramatically with increasing field intensity for Co2Y ferrite and Ni ferrite as shown in Fig.7, while dwell temperatures only increase slightly with increasing field intensity. The ac field intensity in their study is lower than ours. Furthermore, in their study, the heating rates for the Co2Y harder ferrite are at least twice as high as those of the softer Ni-ferrite, which is similar with ours.

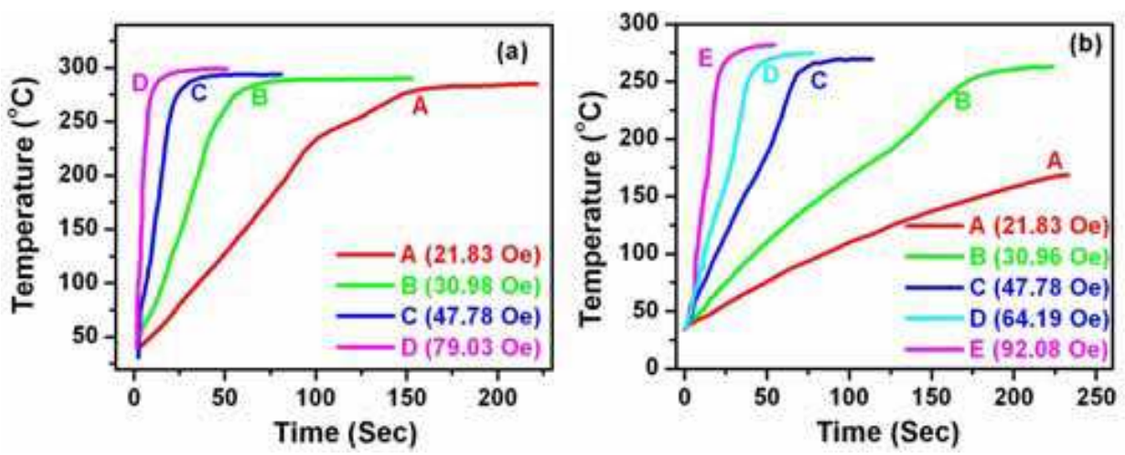
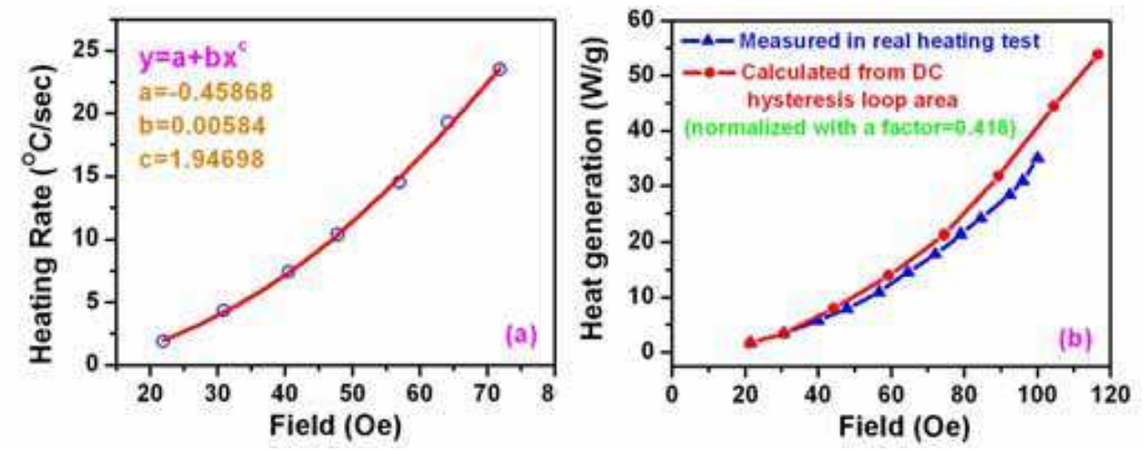


Fig. 7. Heating behaviors of (a) $Co_{1.5}Zn_{0.5}Ba_2Fe_{12}O_{22}$ and (b) $Ni_{0.51}Zn_{0.49}Fe_2O_4$ in a 5.85 MHz ac field[21].

Figure 8 shows the induction heating rate at a fixed temperature (90 °C) as a function of field intensity with 5.85 MHz[21], for one Co2Y ferrite. Note that the heating rate is approximately proportional to the square of the field intensity, as predicted theoretically in expression (4) of hysteresis loss in "Rayleigh" region. By using the correction factor of c_1=0.418, the

theoretical volumetric heat generation rate based on the DC hysteresis loop and the induction field frequency, and the measured volumetric heat generation rate in the sample calculated from the measured heating rates as a function of field intensity are also shown in the Fig8(b).



(a) (b)

Fig. 8. (a) Field dependence of heat generation for $Co_{1.5}Zn_{0.5}Ba_2Fe_{12}O_{22}$ (T=90 °C) in a 5.85 MHz ac field and (b) its comparison with a theoretical curve calculated from the dc hysteresis loop area. [21]

Figure 9 shows induction heating rate as a function of temperature at a fixed field intensity of 72 Oe and frequency of 5.85 MHz, for Co2Y ferrite and Ni ferrite studied by ref [21]. The heating rate shows a maximum at an intermediate temperature between room temperature and the final dwell temperature. We also observed the similar peak of hearting rate at lower frequency and higher field intensity.

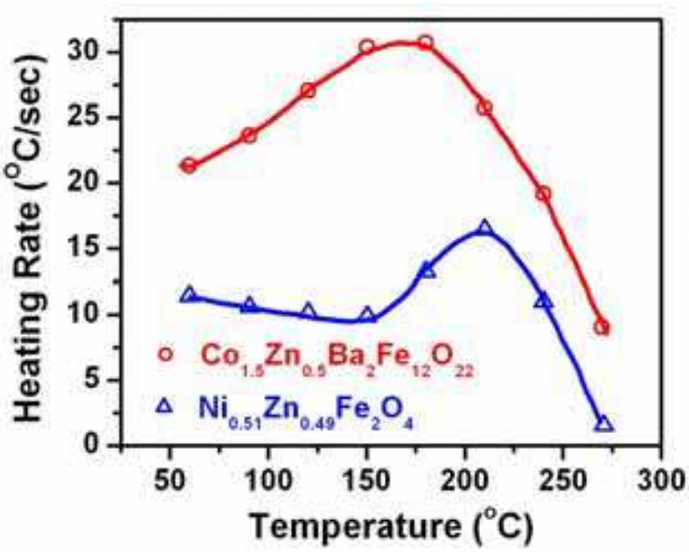


Fig. 9. Temperature dependence of heating rate for $Co_{1.5}Zn_{0.5}Ba_2Fe_{12}O_{22}$ and $Ni_{0.51}Zn_{0.49}Fe_2O_4$ in a 5.85 MHz ac field (72 Oe). [21]

In summary, we investigated the effect of AC magnetic field intensity on magnetic induction heating of three ferrits of $Zn_xFe_3O_4$, $Ni_{1-x}Zn_xFe_3O_4$ and $Co_{1-x}Zn_xFe_3O_4$ nanoparticles. The heating rate increases with increasing intensity of magnetic field and is approximately proportional to the $B_m^{1.6}$, which is consistent with expression (5) for loss at medium and strong magnetic field.

4. Magnetic fluid hyperthermia behavior

Magnetic fluid hyperthermia is based on nanoscale mediators in the form of intravenously injectable colloidal dispersion of magnetic particles. Magnetic nano-particles are dispersed in different liquid carriers to form different magnetic colloid, which can be used to simulate the hypermedia under various bionic or clinic conditions. Since the final temperature of magnetic colloid is limited by liquid boiling point, it is impossible to reach the dwell temperature of net particles (near T_c). Also, the heating rate is not only determined by magnetic particles, but also influenced by many factors such as liquid carrier and so on. Thus magnetic fluid induction heating behaviors is different from that of the net magnetic particles. Fig.10 shows the induction heating curves of the magnetic-water colloid (or suspension) containing $Ni_{0.55}Zn_{0.45}Fe_2O_4$ ferrite nanoparticles with a concentration of the 3mg/ml and the effect of ac field amplitude at a frequency of 71 kHz. It is seen that the heating rate ($\Delta T/\Delta t$) decreases when the liquid temperature increases and finally the temperature approaches a maximum value, dwell temperature. It increases with induction field intensity but the dwell temperature is far below the Curie temperature of the ferrite. This is because the ferrite particles are dispersed in water with boiling point of 100 °C which is the maximum dwell temperature. The dwell temperature geneally refers to the balance between the incoming energy of induction heating and outgoing energy due to evaporation

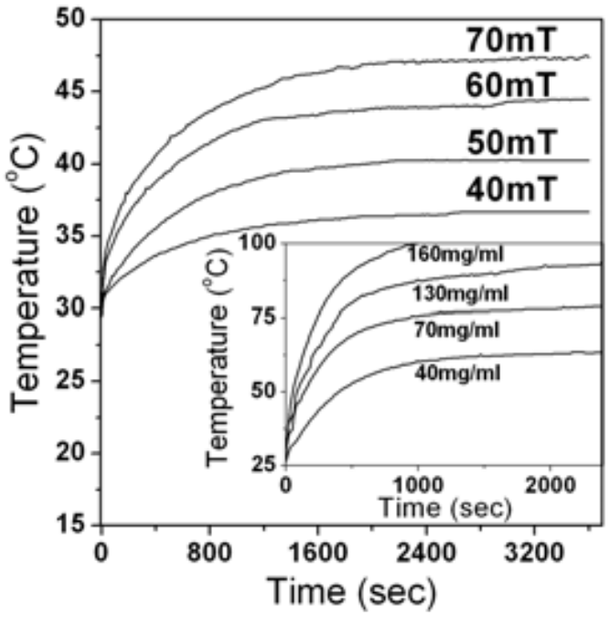


Fig. 10. The induction heating curves of $Ni_{0.55}Zn_{0.45}Fe_2O_4$ ferrite with different concentration at the AC magnetic field of 60 mT.

and heat leakage. The dwell temperature increases with the concentration of the ferrite particles in water and reaches boiling point when the concentration of liquid reaches 160 mg/ml as shown in the inset of Fig.10. The heating rate and dwell temperature increase with increasing field intensity. They are similar to and differ slightly from that in net particles above. The temperature increase of unit mass of magnetic materials due to induction heating in unit time, defined as Specific Absorption Rate (SAR), is determined from the linear temperature rise ΔT of the liquid measured in a time interval Δt after switching on the magnetic field, which is shown by following expression:

$$SAR = n\frac{\Delta T}{\Delta t}$$

where n is the heat capacity of the particle sample, and ΔT/Δt is the slope of the temperature rising data in a time interval. The value of SAR/c obtained from the data in Fig. 10 for Δt =500 sec is shown in Fig. 11. It is seen that the values of ΔT/Δt (SAR/c) are linearly proportional to the square of field strength H^2. The fitted proportional coefficient is SAR/n = ΔT/Δt = 2.8×10^{-4} H^2 (°C/Sec). It differs slightly from that in net particles in Fig.6, and agrees qualitatively with the power loss of magnetic materials in alternating magnetic field according to Rosensweig theory[24]:

$$P = \pi\mu_0\chi H_0^2 f\frac{2\pi f\tau}{1+2\pi f\tau}\infty H_0^2$$

τ is the relaxation time, $\mu_0 = 4\pi\times10^{-7}$ (T mA^{-1}) is the permeability of vacuum and χ is the magnetic susceptibility of the ferrite nanoparticles.

For $Zn_{0.3}Co_{0.7}Fe_2O_4$ nano-ferrite colloid, we also observed that the values of ΔT/Δt (SAR/c) are linearly proportional to the square of field strength as shown in Fig.12. However the different proportional coefficient is obtained by fitting of ΔT/Δt with respect of H^2 for different magnetic colloid.

According the equations of power loss, the theoretical values of SAR should be linearly proportional to the frequency. Dong-Hyun Kim has reported the tested results of

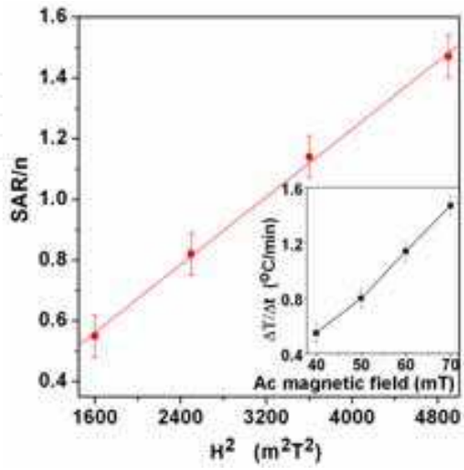


Fig. 11. The SAR/c ~ H^2 curve of the magnetic liquid containing $Ni_{0.55}Zn_{0.45}Fe_2O_4$ ferrite Nanoparticles with a concentration of the 3 mg/ml.

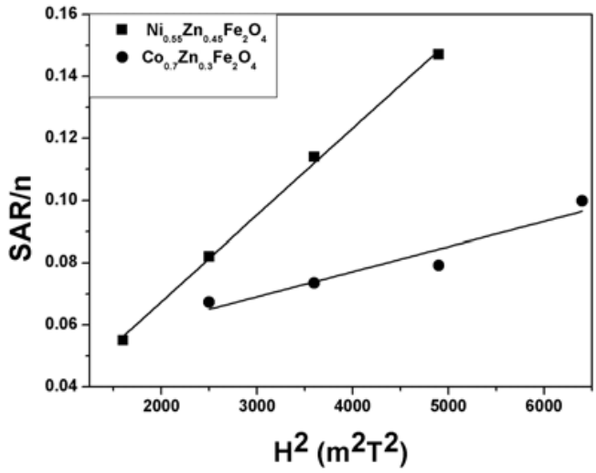


Fig. 12. The SAR/n ~ H^2 curve of the magnetic liquid containing $Ni_{0.55}Zn_{0.45}Fe_2O_4$ and $Zn_{0.3}Co_{0.7}Fe_2O_4$ ferrite nanoparticles with a concentration of the 3 mg/ml.

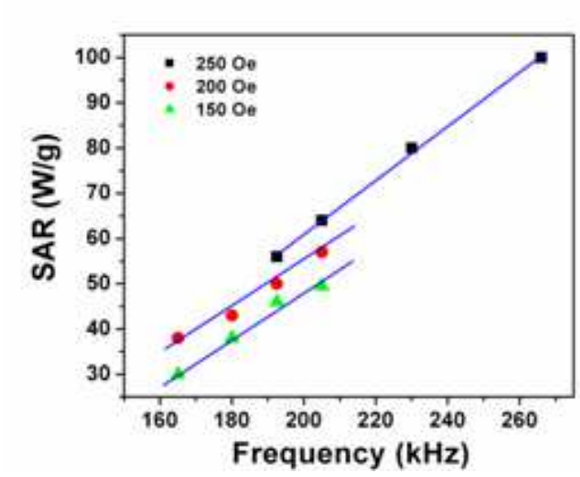


Fig. 13. Frequency of applied ac magnetic fields-dependency of the SAR in the $MnFe_2O_4$ nanoparticles with diameters 10.5 nm[25]

single-crystal $MnFe_2O_4$ nanoparticles with diameters 10.5 nm in three different magnetic field amplitudes. The values of SAR of $MnFe_2O_4$ nanoparticles were found to increase linearly with frequency as shown in Fig.13 [25]. Actually, as the frequency of applied ac magnetic field increases and reaches the resonant frequency of the material, the measured heating rates of net particles does not show a linearly change tendency with frequency, larger than the theoretical heating rates. John Q. Xiao[23] has reported the induction heating rate as a function of frequency at fixed temperature and field strength for a Co2Y ferrite as shown in Fig 14. The dashed line is the theoretical heating rate as a function of frequency and the square dot is the measured heating rate. Note that the measured and theoretical heating rates agree up to around 4.5 MHz, but above that frequency the measured heating rates are higher. This phenomenon is interpreted as due to domain wall resonance effects, and they confirmed the low-field permeability as a function of frequency showed a resonant peak for this material at around 10 MHz.

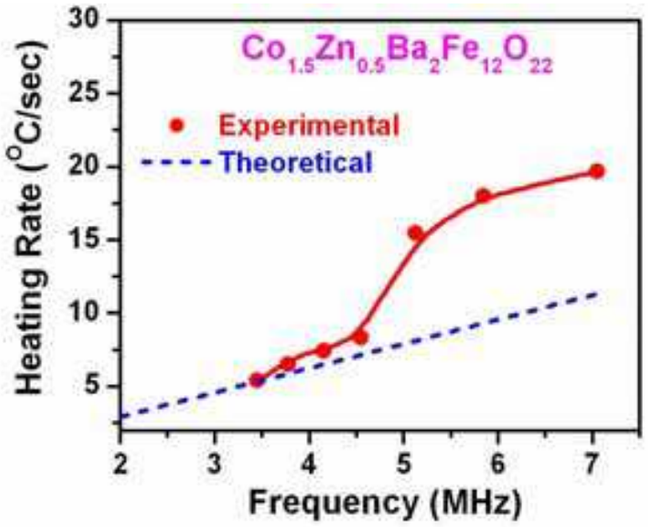


Fig. 14. The experimental and theoretical heating rate dependence of frequency for $Co_{1.5}Zn_{0.5}Ba_2Fe_{12}O_{22}$ at 150 °C and 60 Oe [21]

Fig.15 shows the heating curve and the heating rate of $Ni_{0.5}Zn_{0.5}Fe_2O_4$ fluid with different particle size. It is seen that the dwell temperature and heating rate increase with increasing particle size. The dwell temperature and heating rate reach the maximum (46.5°C and 1.65°C/min) when the particle size increases to critical size from single domain(45nm) to multidomain [26], then they decrease when the particles increase their size further. This tendency agrees with that of coecivity as a function of particle size. The results indicate that the SAR values of magnetite particles are strongly size dependent.

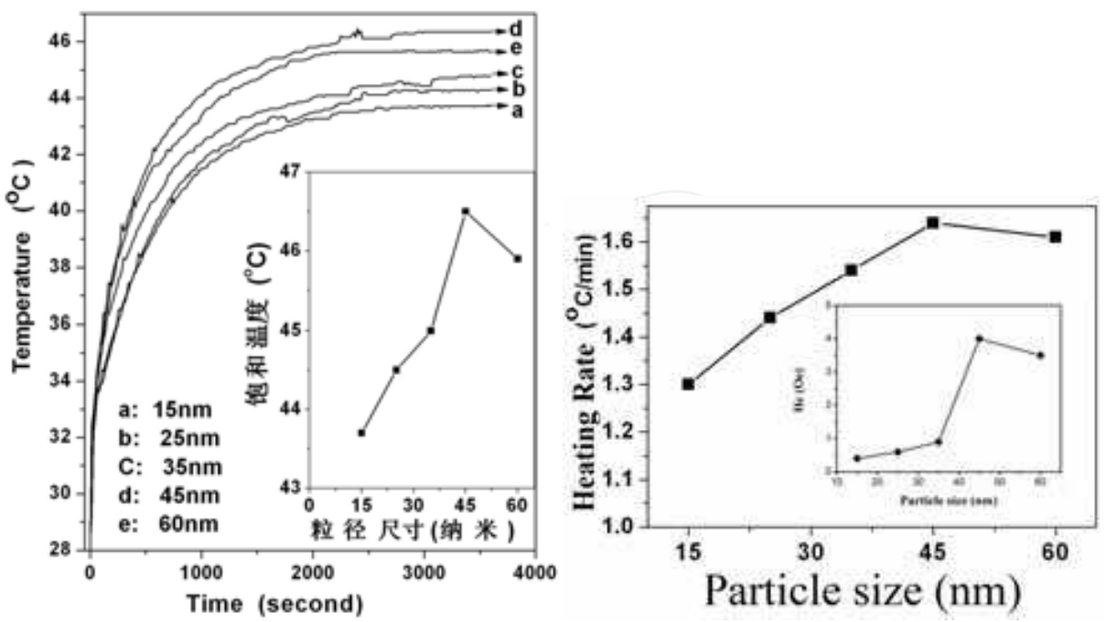


Fig. 15. The heating curve and the heating rate of $Ni_{0.5}Zn_{0.5}Fe_2O_4$ fluid with different particle size.

The power loss of two types of particles was studied by the group of Ning Gu[27]. They reported the specific absorption rate (SAR: specific loss power, defined as the heating power of the magnetic material per gram.) of aqueous suspensions of magnetite particles with different diameters varying from 7.5 to 416nm by measuring the time-dependent temperature curves in an external alternating magnetic field (80 kHz, 32.5 kA/m). For the magnetite particles larger than critical size of single domain, the SAR values increase as the particle size decreases and the coercivity Hc varies with the particle size which matches the variation of SAR values perfectly, indicating that hysteresis loss is the main contribution. For magnetite particles of 7.5 and 13nm which are superparamagnetic, hysteresis loss decreases to zero and, instead, relaxation losses (Neel loss and Brownian rotation loss) dominate, but Brown and Neel relaxation losses of the two samples are all relatively small in the applied frequency of 80 kHz.

Fe_3O_4 is a nery attractive nano-material for bio-applications because it contains only Fe ions which is suitable for body, thus it has been studied extensively [28, 29]. It is shown by studies that the liquid carrier is also an important factor for heating process. The heating rate and the dwell temperature exhibits different values and behavior for different stickiness in colloid. In our experiment, magnetic fluid with concentration of 2 mg/mL was prepared by combining the Fe_3O_4 particles of diameter of 20 nm and deioned water. With the fixed frequency of ac magnetic field at 72 kHz and the varied amplitude of ac fields of 43.1, 54.3, 65.5 mT, we obtained the heating curve of the colloid with Fe_3O_4 particles as shown in Fig. 16. From the left figures in Fig.16, it is seen that the SAR(~$\Delta T/\Delta t$) also shows to be linearly proportional to the square of field amplitude H^2. While in the right figure of Fig.16, it is seen that the more the viscosity of liquid carrier, the higher the dwell temperature and heating rate.

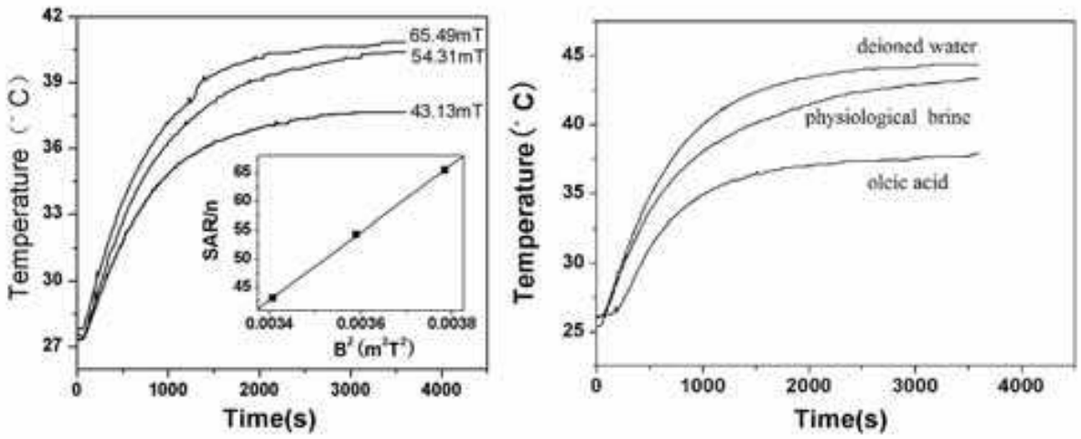


Fig. 16. The induction heating curves of Fe_3O_4 ferrite colloid with the concentration of 2 mg/ml at different amplitudes of AC magnetic field at 72 kHz (left) and in different liquid carrier(right)

On the basis of the physical and biological knowledge, when the magnetic therapy particles are applied for hyperthermia, how to decrease the toxicity and increase the biocompatibility of the particles must be considered. Dong-Lin Zhao et al reported the effect of Fe_3O_4 particles modified with chitosan[30]. the chitosan–Fe_3O_4 particles show multiple fine properties such as non-toxicity, well biocompatibility, biodegradable and anti-bacterial[31]. Babincova et al also reported dextran-magnetite has no measurable toxicity index LD50. [32, 33]

Fig.17 shows that the heating curves of Fe_3O_4 particles with and without SiO_2 shell in the ac magnetic field with 43.1 mT and 72kHz. The average particle size is 30 nm and the shell thickness is about 10 nm. The liquid carrier is deioned water and the concentration of the colloid is about 2 mg/ml. All the test samples have the same volume. From Fig.17 it is seen that the dwell temperature and the heating rate decrease for Fe_3O_4 @ SiO_2 core- shell structures in the colloid compared with Fe_3O_4 particles without shell. This may be partly due to the decrease of the amount of magnetic particle in the colloid with the same volume.

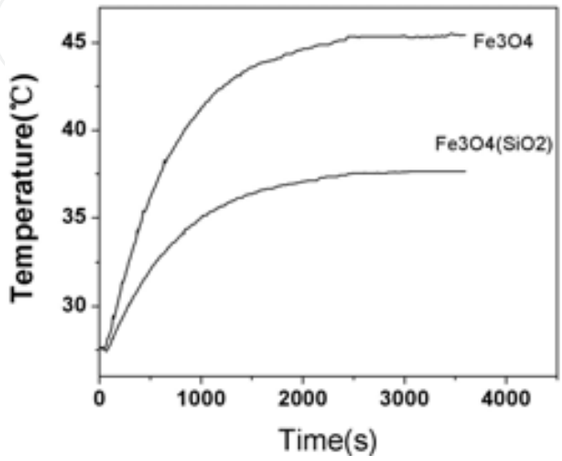


Fig. 17. The heating curves of magnetite with and without silicon oxide shell at ac field.

The heating for ferrofluid in hyperthermia is mainly due to hysteresis loss, Brownian and Neel relaxation loss. The ferrofluid contains the magnetic particles modified with polymer may enhance the Brownian and Neel relaxation loss, which may also increase the SAR value of the ferrofluid. Li-Ying Zhang reported magnetite particles with diameter of 50nm coated by dextran to form homogeneous ferrofluid. The ferrofluid presented a highest SAR value of 75 W/g, which is much higher than 4.5W/g for the 50nm uncoated particles at 55 kHz and 200 Oe. This results indicate that the magnetite particles modified with dextran not only can decrease the toxicity but also can increase the SAR of magnetite ferrofluid[34].

In summary, we report the magnetic induction heating behaviors of magnetic colloids with nanometer particles of ferrite containing Zn and magnetite particles. The SAR increases with increasing intensity of magnetic field and is approximately proportional to the square of the field intensity. They are different from that of the net particles.

5. The closing note

Since the pioneering work of Gilchrist et al. in 1957, magnetic hyperthermia has been the aim of numerous in vitro and in vivo investigations [35, 36], but most of the studies were unfortunately conducted with inadequate animal systems, inexact thermometry and poor AC magnetic field parameters, so that any clinical application was far behind the horizon.

6. Acknowledgment

This work is supported by NBRP (Grant Nos. 2010CB923401 and 2011CB707601), NSFC (Grant Nos. 50472049, 50871029 and 11074034), National Laboratory of Solid State

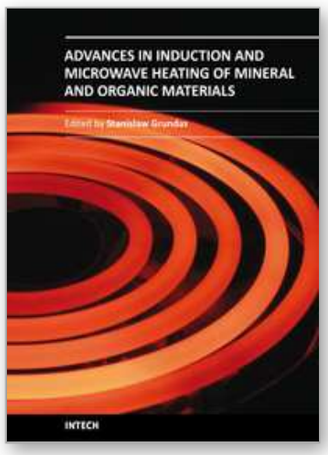
Microstructures at Nanjing University, and Jiangsu Key Laboratory for Design and Manufacture of Micro-Nano Biomedical Instruments, Southeast University.

7. Reference

[1] J. Q. Cao, Y. X. Wang, J. F. Yu, J. Y. Xia, C. F. Zhang, D. Z. Yin, and U. O. Urs O. Häfeli, J. Magn. Magn. Mater., 277, 165 (2004).
[2] D. K. Kim, Y. Zhang, J. Keher, T. Klason, B. Bjelke, and M. Muhammed, J. Magn. Magn. Mater., 225, 256 (2001).
[3] C. H. Dodd, H. C. Hsu, W. J. Chu, P. Yang, H. G. Zhang, Jr J. D. Mountz, K. Zinn, J. Forder, L. Josephoson, R. Weissleder, J. M. Mountz, and J. D. Mountz, J. Immunol. Methods, 256, 89 (2001).
[4] Q. A. Pankhurst, J. Connolly, S. K. Jones, and J. Dobson, J. Phy. D: Appl. Phys., 36, R167 (2003).
[5] P. Tartaj, M. P. Morales, S. Veintemillas-Verdaguer, T. González-Carreño, and C. J. Serna, J. Phy. D: Appl. Phys., 36, R182 (2003).
[6] P. S. Doyle, J. Bibette, A. Bancaud, and J.-L. Viovy, Science, 295, 2237 (2002).
[7] J.-M. Nam, S. I. Stoeva, and C. A. Mirkin, J. Am. Chem. Soc., 126, 5932 (2004).
[8] U. Häfeli, W. Schütt, J. Teller, M. Zborowski, Scientific and Clinical Applications of Magnetic Carriers. New York: Plenum Press, 57, 452 (1997).
[9] W. J. Parak, D. Gerion, T. Pellegrino, D. Zanchet, C. Micheel, S. C. Williams, R. Boudreau, M. A. L. Gros, C. A. Larabell, and A. P. Alivisatos, Nanotechnology, 14, R15 (2003).
[10] A. Jordan, R. Scholz, P. Wust, H. Fakhling, R. Felix, J. Magn. Magn. Mater., 201, 413 (1999)
[11] N. Kawai, A. Ito, Y. Nakahara, M. Futakuchi, T. Shirai, H. Honda, T. Kobayashi, and K. Kohri, The Prostate, 64, 373 (2005)
[12] D. Stoppels, J. Magn. Magn. Mater., 160, 323 (1996).
[13] O. Inoue, N. Matsutani, and K. Kugimiya, IEEE Trans. Magn., 29, 3532 (1993)
[14] J.Smit and H. P. J. Wijn, Ferrites ,
[15] H. Jordan, Elect. Nachr. Techn. 1, 7 (1924).
[16] V. E. Legg, Bell System Tech. J. 15, 39 (1936).
[17] R. M. Bozorth, Ferromagntism, Princeton, N.J. (1951).
[18] R. E. Rosensweig, J. Magn. Magn. Mater., 252, 370 (2002).
[19] M. I. Shliomis, Sov. Phys.-Uspech., 17, 153 (1974).
[20] E. D. Wetzel, B. K. Fink, Y. F. Li, and J. Q. Xiao, Army Sci. Conference, Baltimore, MD (2000).
[21] X. K. Zhang, Y. F. Li, J. Q. Xiao and E. D. Wetzel, J. Appl. Phys. 93, 7124 (2003).
[22] P. M. Levy, S. Zhang, Phys.Rev.Lett., 79 , 5110 (1997)
[23] S. B. Liao, Ferromagnetism (Science Publishing, Beijing, China, 1988), Vol. 3.
[24] R. E. Rosensweig, J. Magn. Magn. Mater., 252, 370 (2002).
[25] D. H. Kim, Y. T. Thai, D. E. Nikles, and C. S. Brazel, IEEE Trans. Magn. 45, 64 (2009)
[26] A. S. Albuquerque, J. D. Ardisson, and W. A. A. Macedo, J. Appl. Phys. 87, 4352 (2000).
[27] M. Ma, Y. Wu, J. Zhou, Y.K. Sun, Y. Zhang, N. Gu, J. Magn. Magn. Mater. 268, 33 (2004)
[28] D.L. Zhao, H. L. Zhang, X. W. Zeng, Q. S. Xia and J. T. Tang, Biomed. Mater., 1, 198 (2006)

[29] L. F. Gamarra, W. M. Pontuschka, J. B. Mamani, D. R. Cornejo, T. R. Oliveira, E. D. Vieira, A. J. Costa-Filho and E. Amaro Jr, J. Phys.: Condens. Matter 21, 115104 (2009)
[30] D.L. Zhao, X.X.Wang, X.W. Zeng, Q.S. Xia, J.T. Tang, J. Alloys Compd., 477, 739 (2009)
[31] J. Zhi, Y.J. Wang, Y.C. Lu, J.Y. Ma, G.S. Luo, React. Funct. Polym. 66, 1552 (2006).
[32] M. Babincova, D. Leszczynska, P. Sourivong and P. Babinec, Med. Hypoth. 54, 177 (2000).
[33] M. Babincova, P. Sourivong, D. Leszczynska and P. Babinec, Med. Hyptoth. 55, 459 (2000).
[34] Li-Ying Zhang, Hong-Chen Gu, Xu-Man Wang, J. Magn. Magn. Mater., 311, 228 (2007).
[35] S. Mornet, S. Vasseur, F. Grasset, E. Duguet. J. Mater. Chem., 14, 2161 (2004).
[36] P. Moroz P, S. K. Jones, B. N. Gray. Int. J. Hyperthermia, 18, 267 (2002)

IntechOpen



Advances in Induction and Microwave Heating of Mineral and Organic Materials

Edited by Prof. StanisÅ‚aw Grundas

ISBN 978-953-307-522-8
Hard cover, 752 pages
Publisher InTech
Published online 14, February, 2011
Published in print edition February, 2011

The book offers comprehensive coverage of the broad range of scientific knowledge in the fields of advances in induction and microwave heating of mineral and organic materials. Beginning with industry application in many areas of practical application to mineral materials and ending with raw materials of agriculture origin the authors, specialists in different scientific area, present their results in the two sections: Section 1-Induction and Microwave Heating of Mineral Materials, and Section 2-Microwave Heating of Organic Materials.

How to reference

In order to correctly reference this scholarly work, feel free to copy and paste the following:

Yi Zhang and Ya Zhai (2011). Magnetic Induction Heating of Nano-Sized Ferrite Particle, Advances in Induction and Microwave Heating of Mineral and Organic Materials, Prof. StanisÅ‚aw Grundas (Ed.), ISBN: 978-953-307-522-8, InTech, Available from: http://www.intechopen.com/books/advances-in-induction-and-microwave-heating-of-mineral-and-organic-materials/magnetic-induction-heating-of-nano-sized-ferrite-particle

INTECH
open science | open minds

InTech Europe
University Campus STeP Ri
Slavka Krautzeka 83/A
51000 Rijeka, Croatia
Phone: +385 (51) 770 447
Fax: +385 (51) 686 166
www.intechopen.com

InTech China
Unit 405, Office Block, Hotel Equatorial Shanghai
No.65, Yan An Road (West), Shanghai, 200040, China
中国上海市延安西路65号上海国际贵都大饭店办公楼405单元
Phone: +86-21-62489820
Fax: +86-21-62489821

© 2011 The Author(s). Licensee IntechOpen. This chapter is distributed under the terms of the Creative Commons Attribution-NonCommercial-ShareAlike-3.0 License, which permits use, distribution and reproduction for non-commercial purposes, provided the original is properly cited and derivative works building on this content are distributed under the same license.

IntechOpen

IntechOpen